Determination of Surface Stress by Seasat-SASS: A Case Study with JASIN Data

W. TIMOTHY LIU

Jet Propulsion Laboratory, California Institute of Technology, Pasadena 91109

W. G. LARGE

National Center for Atmospheric Research,[1] Boulder, CO 80307

(Manuscript received 15 July 1981, in final form 9 September 1981)

ABSTRACT

The values of sea surface stress determined with the dissipation method and those determined with a surface-layer model from observations on F.S. *Meteor* during the Joint Air–Sea Interaction (JASIN) Experiment are compared with the backscatter coefficients measured by the scatterometer SASS on the satellite Seasat. This study demonstrates that SASS can be used to determine surface stress directly as well as wind speed. The quality of the surface observations used in the calibration of the retrieval algorithms, however, is important. This sample of measurements disagrees with the predictions by the existing wind retrieval algorithm under non-neutral conditions and the discrepancies depend on atmospheric stability.

1. Introduction

The Seasat-A Scatterometer System (SASS) was intended to monitor global ocean surface wind (see Born *et al.*, 1979 for a description of Seasat and its instruments). It has long been suggested that the radar backscatter is related to the ocean surface wind (e.g., Moore and Pierson, 1971) and the relation has been demonstrated by using scatterometers on airplanes (e.g., Daley, 1973; Jones *et al.*, 1977), on Skylab (e.g., Ross and Jones, 1977) and on Seasat (e.g., Halberstam, 1980). The Seasat Data Utilization Project has generated ocean surface winds from the entire set of Seasat measurements. The method used is based on the empirical relation

$$\sigma = G(\theta, \phi) + H(\theta, \phi) \log(U_N), \qquad (1)$$

where σ is the backscatter coefficient (normalized radar cross section) in dB; U_N is the equivalent neutral wind at 19.5 m in m s^{-1}; θ is the incidence angle, the angle between the radar beam and nadir; ϕ is the aspect angle, the difference between the wind direction and the radar azimuth. The empirical coefficients G and H are tabulated separately for horizontal and vertical polarizations every 2° in θ and every 10° in ϕ. The version of the G–H table used in the final production of geophysical parameters is called SASS-1 (Schroeder *et al.*, 1981). We will refer to (1) and this G–H table as the Seasat "wind algorithm."

On the theoretical side, it has been postulated that, near vertical incidence, the radar return is governed by physical optics, while away from vertical the return is due to Bragg scattering from short waves tilted by long waves. It has further been postulated that the wave spectrum is affected by surface stress which, in turn, is related to wind speed through a drag law. Since there is no complete and definitive theory on the interaction between short and long waves, and between wind and waves, models developed from the above postulations include parameters that must be adjusted to fit the data. Moore and Fung (1979) and Valenzuela (1978) have reviewed these works.

In many applications, however, the surface stress τ is more relevant than U_N. The surface stress, which represents the momentum exchange between the oceans and the atmosphere, drives the ocean currents and facilitates heat and moisture exchanges by producing turbulent mixings. There are two methods to determine the kinematic stress τ/ρ, where ρ is the surface air density, from SASS measurements. We can rely on the wind algorithm to provide U_N, and then relate U_N to the friction velocity U_* by a neutral drag coefficient, or we can establish a direct relation between σ and U_*, similar to (1). The friction velocity $U_* = (\tau/\rho)^{1/2}$ is the square root of the kinematic stress.

Apart from the uncertainties involving the drag coefficient, there are two concerns regarding the first method: the ocean surface current and the atmospheric stability. These concerns recently were

[1] The National Center for Atmospheric Research is sponsored by The National Science Foundation.

0022-3670/81/121603-09$06.25

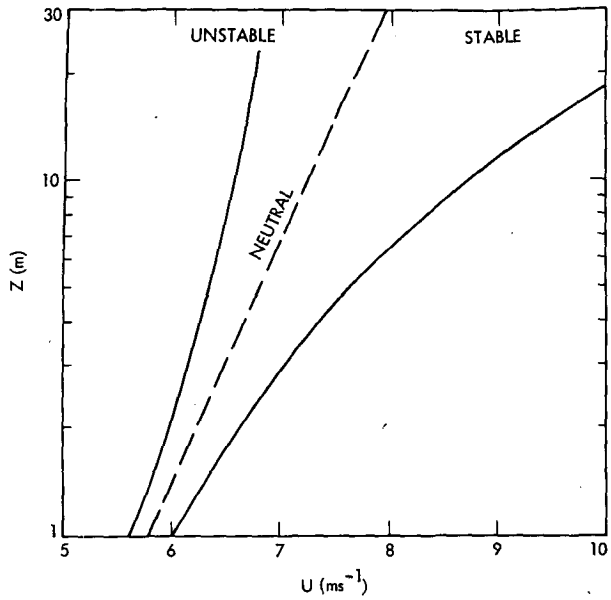

FIG. 1. Vertical profiles of wind in the atmospheric surface layer.

underscored by the study of Weissman *et al.* (1980) who observed sudden changes in radar backscatter at the boundary of the Gulf Stream, a region of sharp contrast in the ocean surface current and atmospheric stability. A uniform wind speed does not always imply a uniform U_* under such circumstances. Since wind speeds are usually measured with respect to a fixed earth, the surface roughness or surface stress depends not on U_N, but on the relative speed $U_N - U_s$. The interfacial velocity U_s is commonly neglected but such action is not always justified.

The velocity profile in the atmospheric surface layer (the layer within 10–50 m from the surface where the fluxes are approximately constant) depends on stability (affected by temperature and humidity stratifications); some typical shapes are sketched in Fig. 1. The wind algorithm relates σ not to the actual wind but to an equivalent neutral wind, supposedly, to eliminate the necessity of accounting for the effects of atmospheric stability. During the compilation of the G–H table for the wind algorithm, methods with different degrees of sophistication have been used to convert wind speeds measured at different heights and under different temperature and humidity stratifications to U_N. To do this correctly, one first has to assume a form of the diabatic profile in the surface layer, which represent a family of curves (Fig. 1). The values of U_* and the roughness parameter (given by the slope at the surface and the z intercept of the curve) from the curve which fits the measurements best are then determined. With these quantities, the neutral profile (straight line) is established and U_N can be evaluated. The degree of success in reducing the stability effect on the wind algorithm remains to be examined. A comprehensive and up-to-date method will be used to evaluate U_N in this study; the mathematical treatment will be presented in Section 2.

The second method for stress determination has been supported by postulations that ocean surface waves are more directly related to surface stress than surface wind and, consequently, σ should correlate with U_* as well as or better than U_N (e.g., Jones *et al.*, 1977). Halberstam (1980) found little difference between the correlation coefficients of σ versus logarithm of U_N and that of σ versus logarithm of U_*. Both his U_N and U_* are derived with a surface-layer model from observed winds. The evaluation of U_N from observed winds has to be preceded by the evaluation of U_*. Therefore, if σ correlates well with U_N, it should also correlate with U_* derived from the same set of observed wind as illustrated in Section 4. A set of independently measured U_* is required to confirm the hypothesis. Brucks *et al.* (1980) have attempted an experimental verification, but there are too few credible measurements of surface stress coincident with backscatter coefficients determinations for a good examination. In this study, a large enough set of U_*, whose determination is independent of U_N, is available for a statistically significant correlation with coincident measurement of σ.

We will use the surface measurements during the Joint Air–Sea Interaction (JASIN) Experiment and coincident SASS measurements at Seasat overpasses to examine the effects of atmospheric stability on the wind algorithm and to study the correlation between σ and U_*.

2. The surface data

a. The WMO reports

The surface measurements for this study were a subset of the data taken throughout the summer of 1978 from F.S. *Meteor* during the JASIN experiment. Meteor was stationed at 59°N, 12.5°W, in the North Atlantic ~400 km northwest of Scotland. Hourly meteorological observations from Meteor were obtained from its WMO reports (weather logs). Wind speeds were measured by a cup anemometer on a port spar and wind directions by a vane on a starboard spar, both at 23 m on the central mast. Wet- and dry-bulb temperatures were measured with an Assman psychrometer at 11 m height. Sea surface temperatures were determined by the bucket method. This set of data was available at the March 1980 Seasat-JASIN Workshop and was incorporated along with additional sets in the compilation of the SASS-1 G–H table.

b. The Gill measurements

An independent set of surface wind data from Gill propeller-vane anemometers also were used. One of the Gill anemometers was placed on a boom at 9 m height ~10 m ahead of the bow. Another Gill anemometer was situated on the ship's center line at 23 m height on the central mast. With the wind direction relative to the ship's heading β within $\pm 60°$ ($\beta = 0$ when the ship headed directly into the wind), measurements at the mast compared favorably with measurements at nearby buoys, while measurements at the boom were ~13% lower after adjusting for height differences. In contrast, with $70° < |\beta| < 120°$, wind speeds from the buoys agreed with those at the boom, but were a few percent higher than those at the mast. The discrepancies are attributed to flow distortion by the ship, which also appeared to reduce the wind speed at the cup anemometer (reported to WMO) by as much as 20% when the wind was from starboard. A nearly continuous Gill wind data set was constructed by using boom measurements when $70° < |\beta| < 120°$ and using the mast measurements when $|\beta| < 60°$. During three satellite passes, only boom measurements were available and $|\beta| < 60°$, so these measurements were used after a 13% correction. There are no data for $60° < |\beta| < 70°$ and for $|\beta| > 120°$.

In a similar fashion, the two Gill anemometers provided a data set for the determination of surface stress and friction velocity from the dissipation method. The dissipation method, the instrumentation, and some previous results have been discussed (Large, 1979; Large and Pond, 1981). In the dissipation method, the dissipation rate is obtained from the velocity spectrum and U_* is related to the dissipation rate through the balance of turbulent kinetic energy. Throughout the JASIN experiment, the dissipation rate was averaged over 20 min periods and the surface stress calculated. Those periods affected by ship maneuvers and radio interference were rejected. The stresses from good periods were averaged to give a representative stress and friction velocity for the hour.

c. The surface-layer parameterization model

From the measurements of wind speed, sea surface temperature, dry- and wet-bulb temperatures, U_N, U_* and the stability parameter $\xi = z/L$, where z is the height and L is the Obukhov length, were also determined with the parameterization model of Liu *et al.* (1979). Essentially, the universal similarity relations in the atmospheric surface layer

$$k(U - U_s)/U_* = \ln(z/z_0) - \psi_U, \qquad (2a)$$

$$k\alpha_H(T - T_s)/T_* = \ln(z/z_T) - \psi_T, \qquad (2b)$$

$$k\alpha_E(Q - Q_s)/Q_* = \ln(z/z_Q) - \psi_Q, \qquad (2c)$$

were used. In these relations, α_H is K_H/K_M and α_E is K_E/K_M at neutral stability, where K_M, K_H and K_E are turbulent diffusivites of momentum, heat and moisture, respectively. The scaling factors U_*, $T_* = -H/(c\rho U_*)$, and $Q_* = -E/(\rho U_*)$ are, by definition, functions of the stress, the heat flux H, and the moisture flux E. The von Kármán constant k, the isobaric specific heat of surface air c, ρ, α_H, and α_E are assumed to be constants. The roughness lengths z_0, z_T and z_Q represent interfacial conditions and have been formulated in terms of U_* and other fluid properties. The stability functions ψ_U, ψ_T and ψ_Q are universal functions of ξ which, in turn, can be expressed in terms of U_*, T_*, Q_*, T, Q and z. The Obukhov length L is defined as

$$L = (T_v U_*^2)/(gkT_{v*}),$$

where

$$T_v = T(1 + 0.61Q),$$

$$T_{v*} = T_*(1 - 0.61Q) + 0.61TQ_*,$$

and g is the acceleration due to gravity. The surface velocity U_s was neglected and the surface humidity Q_s was assumed to be the saturation humidity at the surface temperature T_s. With the measurements of wind speed U (from either the cup or the Gill anemometer), temperature T, specific humidity Q at height z and T_s, the three equations were solved for U_*, H and E. In turn, ξ and z_0 were evaluated. The value of U_N at 19.5 m was determined assuming $\xi = 0$ and substituting the values of z_0 and U_* in (2a). The temperature and humidity profiles (2b) and (2c) affect the velocity profile (2a) through stability. This method of evaluating U_* is equivalent to the use of a drag coefficient which varies with reference height, atmospheric stability and interfacial conditions. A complete description of similarity relations and their solutions has been presented by Liu *et al.* (1979).

In solving (2), z_0 was related to U_* implicitly through a relation between the neutral drag coefficient referenced to 10 m, C_{DN10}, and the wind speed at 10 m, U_{10}:

$$10^3 C_{DN10} = \begin{cases} 1.2, & U_{10} \leq 11 \text{ m s}^{-1} \\ 0.49 + 0.065U_{10}, & U_{10} > 11 \text{ m s}^{-1} \end{cases}$$

This drag formula was determined by Large and Pond (1981) and was found to fit the entire set of wind and stress measurements with the Gill anemometer on Meteor during the JASIN experiment (Large and Pond, 1980). It fits the surface measurements used in this study slightly better than alternate empirical drag formulas by Kondo (1975) and Smith (1980).

3. The satellite data

The satellite data were obtained from the "basic sensor data records" of the Seasat-SASS, at an intermediate step in the satellite data processing, before the wind algorithm is applied to produce U_N. A total of 1070 values of σ were found with centers of surface footprint within 0.5° latitude and 1° longitude from Meteor during the hours of stress measurements. Out of this set of σ values, those with a normalized standard deviation (an indicator of instrumental noise given in the data record) >50% were discarded leaving 925 values of σ corresponding to 84 h of stress measurements. The values of σ were integrated over the footprint areas which vary with the incidence angle, their position on the earth, and whether the satellite is in ascending or descending modes. With this set of data, the footprint areas vary from 729 to 2137 km^2. The distances from the centers of footprint to Meteor vary from 1.6 to 78.5 km. The incident angles vary from 0 to 66°.

The Scanning Multi-channel Microwave Radiometer (SMMR) on Seasat provided additional information for computing the atmospheric attenuation correction for the backscatter. Since only part of the SASS measurements covered the same area as the SMMR measurements, such corrections were available to only 430 values of σ corresponding to 42 h of surface stress measurements.

The backscatter coefficient depends not only on U_* but also on θ, ϕ and polarization. The values of σ obtained during the JASIN experiment must be converted to a reference incident angle θ_r and a reference aspect angle ϕ_r for each polarization, before they can be correlated with U_*. Most of the data were converted by

$$\sigma = \sigma_m R$$

and

$$R = \sigma_a(\theta_r, \phi_r, U_m)/\sigma_a(\theta_m, \phi_m, U_m),$$

where subscript m refers to measured value and subscript a refers to values determined by the wind algorithm. The effect of any error is greatly exaggerated by this method of conversion when the denominator of R approaches zero. For a small amount of data for which $R > 1.5$ or $R < 0.5$, an alternate formula for conversion was adopted:

$$\sigma = \sigma_m + D$$

and

$$D = \sigma_a(\theta_r, \phi_r, U_m) - \sigma_a(\theta_m, \phi_m, U_m).$$

The entire set of σ were converted by this method to form data set A. The subset with atmospheric attenuation correction were converted separately to form set B. The reference angles are $\theta_r = 40°$ and $\phi_r = 180°$ in both cases.

The described method of conversion depends on the wind algorithm. An alternate method was used to minimize such dependence. To reduce interpolation in θ, the values of σ were divided into eight bins, each 10° wide in θ, centered on $\theta_r = 25, 35, 45$ and 55° for each polarization. Those with $\theta < 20°$ and $\theta > 60°$ were discarded. The values in each bin were converted to the values at θ_r at the same aspect angle. To eliminate the necessity of interpolation in ϕ, the values of σ from orthogonal beams were averaged. This makes use of the property that σ is approximately dependent on $\cos(2\phi)$ (see Moore and Fung, 1979) and the average of σ measured by orthogonal beams is approximately independent of ϕ. This method was applied to the entire set of σ to form set C.

4. Relating backscatter coefficient and friction velocity

In Figs. 2, 3 and 4, the logarithm of U_* (m s^{-1}) determined by the dissipation method is plotted versus the hourly averages of the converted σ (dB) from sets A, B and C, respectively. The solid lines are the linear regressions. Considering an expected 10% uncertainty in U_*, all data exhibit reasonable correlations. To estimate the amount of scatter, U_* were estimated from σ through the linear regressions in Fig. 3. The root-mean-square (rms) differences between these values of U_* and those determined by dissipation method were found to be 0.03 m s^{-1} or 12% of the averaged U_* for both polarizations. In comparing σ, which is integrated over area, and U_*, which is integrated over time, Taylor's hypothesis is assumed. The validity of Taylor's hypothesis in approximately the same area during the JASIN experiment has been investigated by Ishida (1980). With the absence of sharp weather variations during the period and within the area of interest, the hypothesis appeared to be justified.

The regressions were obtained for three sets of σ and five sets of surface parameters: U_*(DISS), U_N(GILL), U_*(GILL), U_N(CUP), U_*(CUP). Besides U_*(DISS) which is the friction velocity determined with the dissipation method, the other parameters were evaluated with the surface-layer model. These four parameters are the equivalent neutral wind and the friction velocity from either the Gill wind or the cup wind as indicated in the parentheses. The sea surface temperature, the dry- and wet-bulb temperatures from the WMO reports were used in the evaluation of all four parameters. The correlation coefficients are listed in Table 1. The number of hours of data used in each regression N are also shown.

The correlation coefficients of $\log(U_*)$ versus σ and the coefficients of $\log(U_N)$ versus σ, with both U_* and U_N derived with the surface-layer model (from either the Gill wind or the cup wind) are almost identical. The results can be explained by considering the correlation coefficient γ_{XY} of two

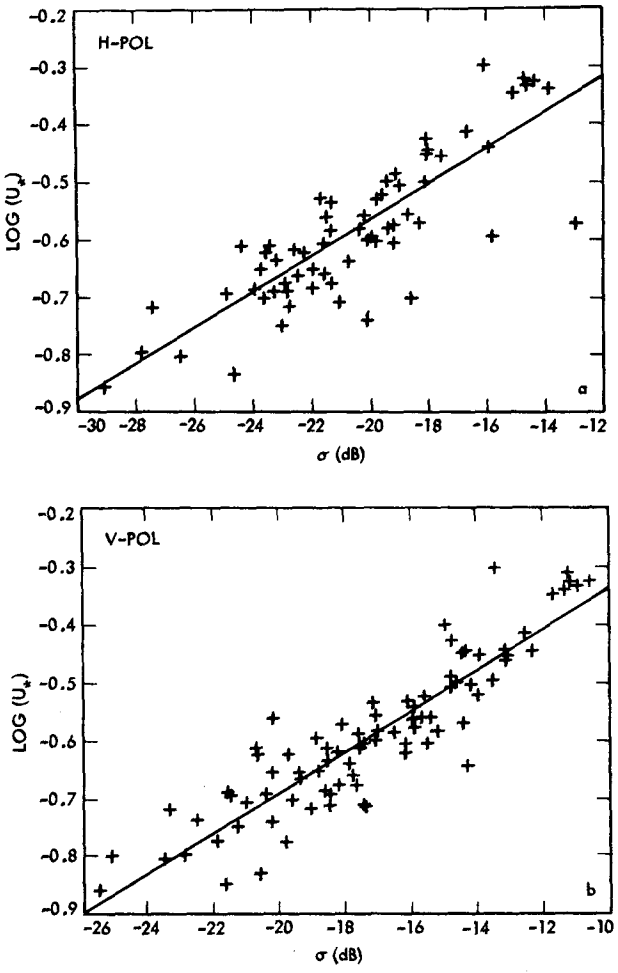

FIG. 2. Logarithm of the friction velocity U_* determined with the dissipation method versus the backscatter coefficient σ for (a) horizontal polarization and (b) vertical polarization. The backscatter coefficients are converted to an incidence angle of 40° and an aspect angle of 180°. They are not corrected for atmospheric attenuation.

sets of numbers X and Y. If a new set of numbers Z is generated from Y by a linear relation, then γ_{XY} will be equal to γ_{XZ}. When both U_N and U_* are derived from the same set of observed wind speeds with the same drag law or surface-layer profile, each pair of U_N and U_* is perfectly related. By definition, $U_*/U_N = C_{DN}^{1/2}$. The neutral drag coefficient C_{DN} is independent of atmospheric stratifications; it varies only slightly with wind speed for most drag laws or surface layer models. For a range of moderate wind speeds, it is approximately constant and $\log(U_*)$ and $\log(U_N)$ are linearly related: $\log(U_*) = 0.5 \log(C_{DN}) + \log(U_N)$. Therefore, the correlation coefficients should be approximately equal. A set of independently measured U_*, whose relation with U_N is affected by secondary physical processes such as sea state and sea spray, is required for meaningful comparison. The set of U_* determined with the dissipation method was intended for this purpose.

The coefficients for U_*(DISS) are generally higher than those for U_N(CUP) but differ little from those for U_N(GILL). Since the coefficients for U_N(GILL) are higher than those for U_N(CUP), the results are probably indications of flow distortion at the cup anemometer rather than the processes of wind-wave coupling. The coefficients for U_*(GILL) are higher than those for U_N(GILL) when the data set is small ($N < 10$), the coefficients for the data with atmospheric attenuation correction (especially for horizontal polarization) are higher than those without correction and those with vertical polarization are generally higher than those with horizontal polarization. However, considering the sample sizes, these small differences are not statistically significant. In Fig. 4a there is a sudden slope change and an increase in scatter at $\theta = 45°$. The physical reason, if there is any, requires further investiga-

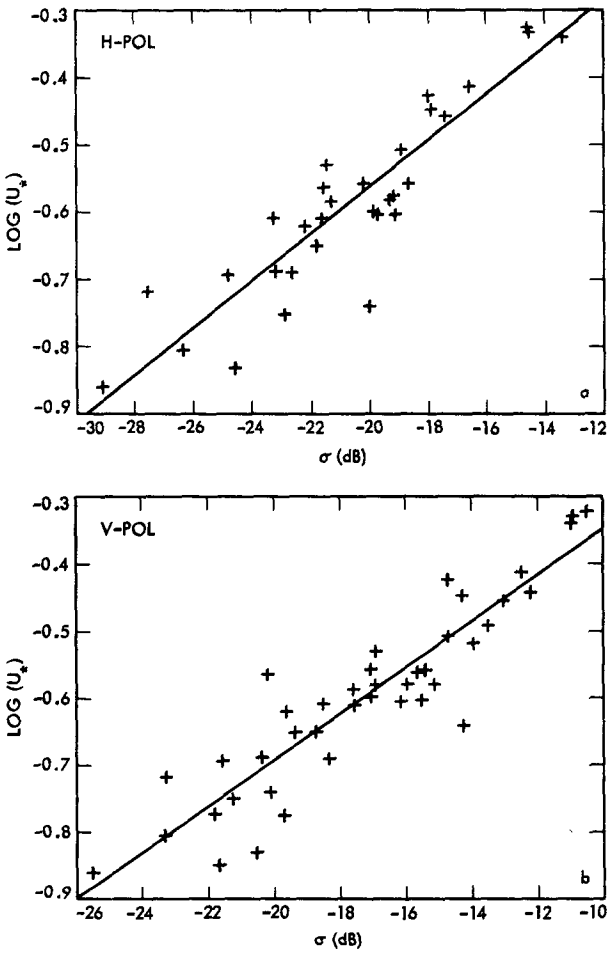

FIG. 3. As in Fig. 2 except that the backscatter coefficients are corrected for atmospheric attenuation.

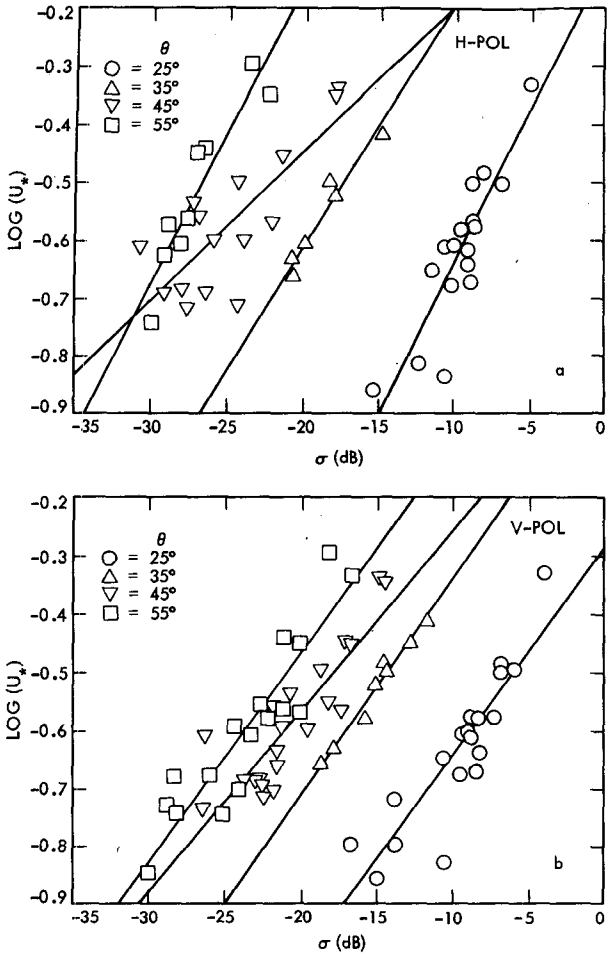

FIG. 4. As in Fig. 2 except that the backscatter coefficients are averaged for orthogonal beams at various incident angles.

tion. Other than this, there is no obvious preference for incidence angle.

The slopes of the regressions, in the form of power indexes a and b in the expressions $\sigma\alpha U_N^a$ and $\sigma\alpha U_*^b$, are given in Table 2. The values of a and b vary with incident angle and polarization, with a typical value of 2.4 at moderate to high incidence angles. Monahan and Muircheartaigh (1980) suggested that the whitecap coverage increases with wind speed raised to a power of 3.4 over similar range of wind speed. The effects of whitecap and other factors such as wind fetch and surface film are outside the scope of this study.

TABLE 1. Correlation coefficients of σ versus surface parameters.

	Pol	θ_r	N	Gill U_N	Gill U_*	Cup U_N	Cup U_*	Dissipation U_*
A	*H*	40	64	0.86	0.86	0.75	0.75	0.83
	V	40	84	0.93	0.92	0.84	0.84	0.90
B	*H*	40	31	0.91	0.91	0.78	0.79	0.91
	V	40	41	0.93	0.93	0.83	0.83	0.91
C	*H*	25	17	0.91	0.91	0.81	0.82	0.89
	H	35	6	0.79	0.79	0.94	0.94	0.98
	H	45	15	0.83	0.84	0.72	0.73	0.79
	H	55	9	0.83	0.85	0.81	0.81	0.93
	V	25	19	0.90	0.90	0.72	0.73	0.87
	V	35	8	0.81	0.81	0.68	0.68	0.99
	V	45	21	0.90	0.90	0.86	0.86	0.87
	V	55	17	0.92	0.92	0.90	0.90	0.92

5. The effects of atmospheric stability

In order to examine the effects of atmospheric stability on the wind algorithm, the algorithm-derived backscatter coefficients were compared with those obtained with the dissipation method. Let σ_m and U_m be the backscatter coefficient observed by Seasat-SASS and the corresponding equivalent neutral wind at 19.5 m determined from surface observations. From the wind algorithm, a backscatter coefficient σ_a can be derived from U_m and a wind speed U_a can be derived from σ_m, such that

$$\sigma_a = G + H \log(U_m) \tag{3}$$

and

$$\sigma_m = G + H \log(U_a). \tag{4}$$

Combining (3) and (4), we have

$$\log(U_a/U_m) = (\sigma_m - \sigma_a)/H. \tag{5}$$

This relates the differences in wind speeds to that in backscatter coefficients.

In Fig. 5, the ratio σ_a/σ_m is plotted versus the stability parameter for horizontal and vertical polarizations. The ratio is averaged over bands equal to one-tenth in ξ. Out of 925 values, four outliers with exceptionally large values were discarded before averaging. The error bar equivalent to one standard deviation and the number of data in each band also are shown. There appears to be a dependence of the ratio on atmospheric stability. Near neutral condi-

TABLE 2. Values of a and b from regressions: $\sigma\alpha U_N^a$ and $\sigma\alpha U_*^b$.

	Pol	θ_r	N	a	b
A	*H*	40	64	2.2	2.2
	V	40	84	2.1	2.3
B	*H*	40	31	2.1	2.3
	V	40	34	2.4	2.4
C	*H*	25	17	1.4	1.5
	H	35	6	3.7	2.3
	H	45	15	2.7	2.5
	H	55	9	1.5	1.7
	V	25	19	2.2	2.2
	V	35	8	3.3	2.6
	V	45	21	2.4	2.4
	V	55	17	2.4	2.4

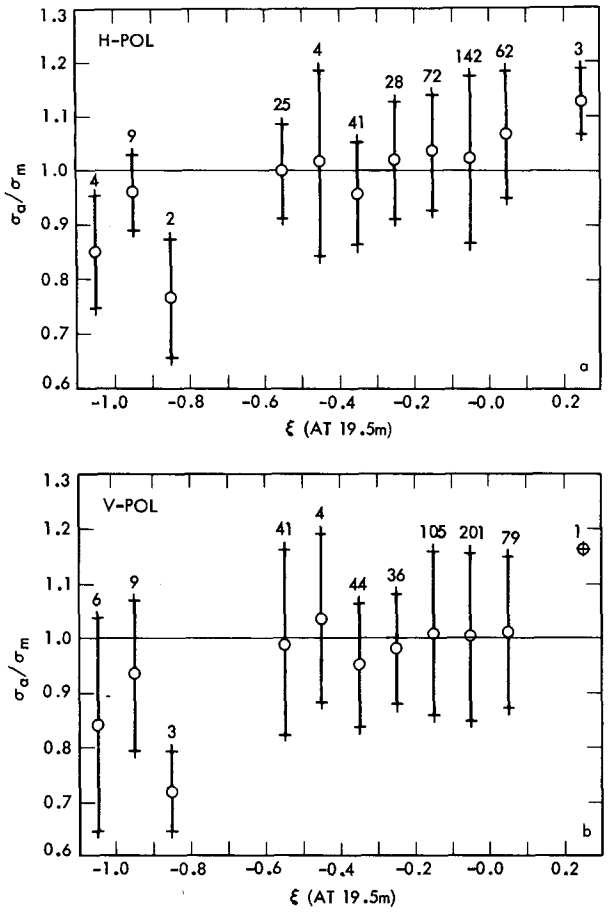

FIG. 5. The ratio of algorithm-determined backscatter coefficient σ_a to the measured value σ_m versus stability parameter ξ for (a) horizontal polarization, and (b) vertical polarization. The Seasat wind-retrieval algorithm is used.

tions ($\xi = 0$), the algorithm approximates the backscatter coefficients closely. However, overestimation and underestimation of the absolute values occurs under stable ($\xi > 0$) and unstable ($\xi < 0$) conditions, respectively. As an example, at $\xi = -1$ the band averages indicate a value of ~0.85 for the ratio, or σ_a 15% smaller than σ_m in absolute magnitude. Similarly, $\sigma_a - \sigma_m$ can be determined to be 1.6 and 2.1 for horizontal and vertical polarizations respectively for the same set of data. The value of H varies with θ, ϕ and polarization. For a typical value of $H = 20$, U_a/U_m is approximately 0.8 for both polarizations according to (5). Therefore, under moderately unstable conditions, we would expect an error on the order of 20% in the SASS-derived wind speed.

Attempts to use different values of empirical constants in the formulations of ψ_U, ψ_T, ψ_Q in (2a, b, c) in the determination of ξ resulted only in slight shifts or compressions of the abscissas of Fig. 5. Changing the bandwidth did not significantly change the stability dependence trends either. The data used here cover only a moderate range of stability generally encountered in the open ocean. The temperature difference between the surface and 11 m height ranges from −0.7° to 2.5°C and the difference in humidity ranges from −0.3 up to 3.2 g kg^{-1}. If the trends can be extrapolated, larger error would be encountered under stronger instability. Finally, a caveat appears warranted: the distribution of data is uneven, with most data concentrated in near-neutral bands. The trend of stability dependence is governed by a comparatively small amount of data.

The possibility of reducing or even eliminating the stability effects by careful calibration of the retrieval algorithm is demonstrated in Fig. 6. A linear regression of the adjusted backscatter coefficients σ_m from Set A and the logarithm of the U_N(GILL) was obtained as discussed in Section 4. This is equivalent to the determination of new values of G and H of the wind algorithm at the reference θ and ϕ. In Fig. 6 σ_a is evaluated from the U_N(GILL) with this new algorithm. Residual stability dependence of the ratio σ_a/σ_m is expected because σ_m

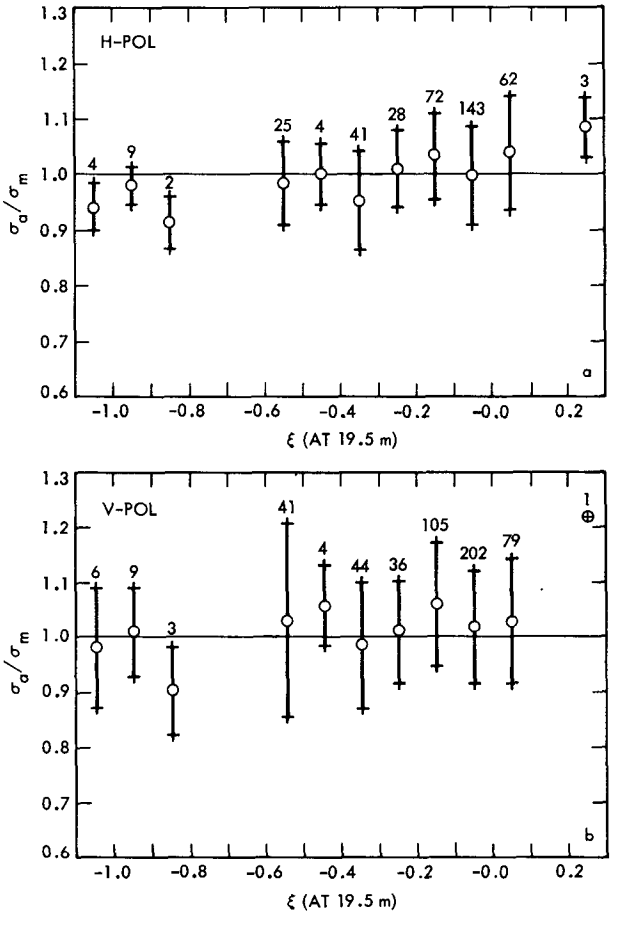

FIG. 6. As in Fig. 5 except that algorithm based on this set of data is used instead of the Seasat wind-retrieval algorithm.

is adjusted to the reference values with the Seasat wind algorithm but the stability effects are much reduced when compared with Fig. 5. Similar reduction in the stability effects were observed when the U_*(DISS) was used instead of U_N(GILL).

6. Conclusion

For the first time, a large enough set of U_*, not derived from the mean wind, was used to demonstrate the correlation between the radar backscatter and the sea surface stress. This case study shows no significant difference between the correlation of σ vs U_N and σ vs U_*. The effects of flow distortion on the surface wind observations produced more significant differences. However, this study covers only a very moderate stability range and is under conditions of negligible ocean surface current. A study under more extreme conditions (e.g., over the Gulf Stream) will be valuable.

Only about half of the SASS data were corrected for atmospheric attenuation which depends mainly on the water content in the atmosphere. Over the JASIN experimental area, the correction only made a slight difference in the correlation between σ and U_*. Larger effects would be expected in areas with higher atmospheric water content, such as in the tropical areas. In such cases, the problem of obtaining information for the attenuation correction has to be addressed. This may involve covering the SASS footprints with an instrument like SMMR in any future experiment with the SASS.

This study demonstrated the stability-dependent discrepancy between predictions by the wind algorithm and the sample measurements. It is possible that σ is affected by a stability-dependent mechanism, yet unidentified and not accounted for in (1). Otherwise, the stability effects have not been completely eliminated from the wind speeds used in the compilation of the G–H table. The study also shows that the stability effects can be reduced or eliminated by recalibration of the wind algorithm. A uniform and carefully designed procedure should be used to prepare all the equivalent neutral winds used in such a process. In order to achieve the 10% or ± 2 m s^{-1} accuracy in wind speed as specified for SASS, the effect of atmospheric stability should not be taken lightly.

The atmospheric stability depends on both heat and moisture fluxes. Methods to determine these fluxes from satellite measurements have been suggested (e.g., Liu, 1981), but these methods require further studies and testing. Since there is no operational method to estimate atmospheric stability from satellite data at present, a geophysical algorithm free from the influence of stability will be valuable for the utilization of the SASS.

In deciding the surface parameter in terms of which the scatterometer measurements should be interpreted, the expedience in geophysical applications should be considered. In the determination of air–sea exchanges in momentum, heat and moisture, much computational effort would be saved and the uncertainty in one of the parameterization schemes (from U_N to U_*) would be eliminated if U_* instead U_N can be determined directly from the scatterometer measurements (Liu, 1981; Kraus, 1981). Direct correlation between σ and U_* also would reduce or eliminate the problems of surface current and atmospheric stability.

This data set alone is not large enough for recalibrating the existing wind algorithm or for compiling an operational algorithm to determine U_* for the whole range of θ and ϕ. The results of this study, however, exemplify and justify such efforts in future applications of the scatterometer.

Acknowledgments. This study was performed at Jet Propulsion Laboratory, California Institute of Technology under NASA contract NAS7-100. Members of the Seasat Data Utilization Project at JPL kindly provided information on the Seasat data. The WMO reports were obtained from the Institute of Oceanographic Science (IOS), Wormley, England.

The Gill anemometers and the dissipation system were part of the JASIN program of the University of British Columbia with Dr. S. Pond, supported by the U.S. office of Naval Research (Contract N00014-76-C-0046 under project 083-207) and by the National Research Council of Canada (Grant A8301). The data from the Gill anemometers were analysed at the IOS.

REFERENCES

Born, G. H., J. A. Dunne and D. B. Lame, 1979: Seasat mission overview. *Science*, **204**, 1405–1406.

Brucks, J. T.,W. L. Jones and T. D. Leming, 1980: Comparison of surface wind stress measurements: airborne radar scatterometer versus sonic anemometer. *J. Geophys. Res.*, **85**, 4967–4976.

Daley, J. C., 1973: Wind dependence of radar sea return. *J. Geophys. Res.*, **78**, 7823–7833.

Halberstam, I., 1980: Some considerations in the evaluation of Seasat-A scatterometer (SASS) measurements. *J. Phys. Oceanogr.*, **10**, 623–632.

Ishida, H., 1980: Analysis of meteorological observations from an array of buoys during JASIN. M.S. thesis, Oregon State University, Corvallis, 63 pp.

Kondo, J., 1975: Air–Sea bulk transfer coefficients in diabatic conditions. *Bound-Layer Meteor.*, **9**, 91–112.

Kraus, E. B., 1981: The latent and sensible heat flux. *Proc. Workshop on Application of Existing Satellite Data to the Study of the Ocean Surface Energetics*, C. Gautier, Ed., University of Wisconsin Press, 17–28.

Large, W. G., 1979: The turbulent fluxes of momentum and sensible heat over the open sea during moderate to strong winds. Ph.D. thesis, Institute of Oceanography and Dept. of Physics, University of British Columbia, 180 pp.

——, and S. Pond, 1980: JASIN surface fluxes. *JASIN News*, **21**, Unpublished Manuscript.

——, and ——, 1981: Open-ocean momentum flux measurements in moderate to strong winds. *J. Phys. Oceanogr.*, **11**, 324–336.

Liu, W. T., K. B. Katsaros and J. A. Businger, 1979: Bulk parameterization of air–sea exchanges of heat and water vapor including the molecular constraints at the interface. *J. Atmos. Sci.*, **36**, 1722–1735.

Liu, W. T., 1981: Evaluation of parameterization models for determinating air–sea exchanges in heat and momentum from satellite data. *Proc. Workshop on Applications of Existing Satellite Data to the Study of the Ocean Surface Energetics*. C. Gautier, Ed., University of Wisconsin Press, 35–42.

Jones, W. L., L. C. Schroeder and J. L. Mitchell, 1977: Aircraft measurements of the microwave scattering signature of the ocean. *IEEE Trans. Antennas Propag.*, **AP-25**, 52–61.

Monahan, E. C., and I. O. Muircheartaigh, 1980: Optimal power-law description of oceanic whitecap coverage dependence on wind speed. *J. Phys. Oceanogr.*, **10**, 2094–2099.

Moore, R. K., and A. K. Fung, 1979: Radar determination of winds at sea. *Proc. IEEE*, **67**, 1504–1521.

——, and W. J. Pierson, 1971: Worldwide oceanic wind and wave predictions using a satellite radar-radiometer. *J. Hydronaut.*, **5**, 52–60.

Ross, D., and W. L. Jones, 1977: On the relationship of radar backscatter to wind speed and fetch. *Bound-Layer Meteor.*, **13**, 151–163.

Schroeder, L. C., D. H. Boggs, G. Dome, I. M. Halberstam, R. K. Moore, W. J. Pierson and F. W. Wentz, 1981: The relationship between wind vector and normalized radar cross section used to derive Seasat-A satellite scatterometer winds. Submitted to *J. Geophys. Res.*

Smith, S. D., 1980: Wind stress and heat flux over the ocean in gale force winds. *J. Phys. Oceanogr.*, **10**, 709–726.

Valenzuela, G. R., 1978: Scattering of electromagnetic waves from the ocean. *Surveillance of Environmental Pollution and Resources by Electromagnetic Waves*, T. Lund, Ed., D. Reidel, 199–226.

Weissman, D. E., T. W. Thompson and R. Legeckis, 1980: Modulation of sea surface radar cross section by surface stress: wind speed and temperature effects across the Gulf Stream. *J. Geophys. Res.*, **85**, 5032–5042.